Estuarine, Coastal and Shelf Science 332 (2026) 109745

Contents lists available at ScienceDirect

Estuarine, Coastal and Shelf Science

journal homepage: www.elsevier.com/locate/ecss

An observational study of saltwater intrusion into the Yellow River estuary

Yunan Hu [a,b], Xinyu Guo [c], Yucheng Wang [d], Tao Zou [e], Fangguo Zhai [f], Xiaojie Yu [a,b,*]

[a] Key Laboratory of Marine Environment and Ecology, College of Environmental Science and Engineering, Ocean University of China, Ministry of Education, Qingdao, 266100, China
[b] Laboratory for Marine Ecology and Environmental Science, Qingdao Marine Science and Technology Center, Qingdao, 266237, China
[c] Center for Marine Environmental Studies, Ehime University, Matsuyama, 790-8577, Japan
[d] Laoshan Laboratory, Qingdao, 266237, China
[e] Key Laboratory of Coastal Zone Environmental Processes and Ecological Remediation, Yantai Institute of Coastal Zone Research, Chinese Academy of Sciences, Yantai, 264003, China
[f] College of Oceanic and Atmospheric Sciences, Ocean University of China, Qingdao, 266100, China

ARTICLE INFO

Keywords:
Saltwater intrusion
Yellow river estuary
Field survey
Tidal variation
Wind

ABSTRACT

This research examines the phenomenon of saltwater intrusion in the Yellow River estuary (YRE) through utilization of shipboard surveys and mooring investigations. Hydrographic data were gathered in May and October 2023 to elucidate the relationship between saltwater intrusion in YRE and various factors, including tides, winds, and river discharge. The fortnightly cycle of the diurnal tide within the estuary is controlled by the declination of the moon above and below the equator, rather than by the lunar phase, as is the case in a semidiurnal system. The spring tides occur two days after the maximum lunar declination and neap tides occur two days following the zero value of lunar declination. Surface salinity within estuary demonstrates semidiurnal fluctuations, with an initial peak occurring prior to high tide and a subsequent peak during early ebb phase. The earlier peak is attributed to interplay between upstream tidal currents and downstream fluvial flow, while the later peak is likely influenced by saltwater which has intruded into river channel. Conversely, bottom salinity exhibits diurnal variations, as seawater is driven into and out of river channel by diurnal tidal currents. The peak salinity levels in the estuary correspond to fortnightly variations in water elevation, indicating stronger intrusion during spring tides than in neap tides. Additionally, strong northeasterly winds can enhance saltwater intrusion; however, intrusion is hindered once the winds subside in following day. This phenomenon of wind-induced hindrance has not been previously documented and may be attributed to significant accumulation of freshwater within the river due to northeasterly winds. Overall, saltwater intrusion is more intense during winter and spring than in summer and autumn.

1. Introduction

Saltwater intrusion is a prevalent phenomenon in estuaries where freshwater and seawater converge, playing a crucial role in the estuarine density gradient, circulation, and mixing processes. It significantly alters the transport of sediments, pollutants, and waterborne materials (Hao et al., 2024; MacCready and Geyer, 2010; Xing et al., 2013), as well as the distribution of estuarine vegetation and ecosystem habitats (Neubauer, 2013). Enhanced saltwater intrusion can disrupt freshwater intake for domestic and industrial uses in surrounding areas (Liu et al., 2019), and may even threaten the survival of certain aquatic species within the estuary, such as *Leuciscus aspius* (Kujawa and Piech, 2022; Goe et al., 2025). Consequently, this can lead to substantial economic losses and degradation of transitional habitats (Tully et al., 2019; Zhu et al., 2020). Therefore, saltwater intrusion has long been a globally significant research focus, attracting extensive scholarly attention.

The pattern of saltwater intrusion is significantly influenced by a variety of critical factors, including riverine input, tidal movements, wind patterns, estuarine topography, climatic changes (such as storm events and sea level rise), and anthropogenic activities (Chen et al., 2016; Liu et al., 2007; Loc et al., 2021; Lyu and Zhu, 2019; Perales-Valdivia et al., 2018; Qiu and Zhu, 2015; Savenije, 2012; Veerapaga et al., 2019). Wherein, riverine input plays a pivotal role in determining the extent of saltwater intrusion. Specifically, river discharge serves to

* Corresponding author. Key Laboratory of Marine Environment and Ecology, College of Environmental Science and Engineering, Ocean University of China, Ministry of Education, Qingdao, 266100, China.
E-mail address: yxj@ouc.edu.cn (X. Yu).

https://doi.org/10.1016/j.ecss.2026.109745
Received 21 October 2025; Received in revised form 21 January 2026; Accepted 30 January 2026
Available online 31 January 2026

mitigate the upstream transport of saltwater within an estuary, and it is widely accepted that saltwater intrusion is inversely correlated with riverine input (Liu et al., 2007; Wang et al., 2019). Numerous studies have indicated that the saltwater intrusion length, typically defined by the 2-PSU isohaline, adheres to a power law relationship with river discharge, where the power dependence coefficient varies in a wide range in different estuarine conditions (Abood, 1974; Monismith et al., 2002; Ralston et al., 2010). Furthermore, the sensitivity of saltwater intrusion length to fluctuations in river discharge will increase during high flow conditions, with a smaller coefficient compared to low flow scenarios (Ralston et al., 2010).

Tides exert a significant influence on saltwater intrusion across various timescales. On intra-tidal timescales, saltwater intrudes into the estuary during flood-tide periods and is expelled from the estuary during ebb-tide periods. As a result, the maximum salt intrusion occurs at flood slack, while the minimum salt intrusion is observed at ebb slack. The fortnightly fluctuations in tidal range modulate the extent of saltwater intrusion, exhibiting distinct patterns in estuaries with different salt transport mechanisms (Payo-Payo et al., 2022). Stronger saltwater intrusion is typically observed during neap tides in estuaries characterized by exchange flow (Gong and Shen, 2011), whereas in estuaries where tidal dispersion dominates, larger intrusion lengths are noted during spring tides (Wu et al., 2010). Additionally, numerical modelling conducted by Qiu et al. (2012) indicates that the seasonal variability of tides enhances saltwater intrusion in the Changjiang estuary, with the most significant tidal range occurring during the spring tides in March.

In addition to runoff and tidal influences, winds also play a significant role in the alteration of saltwater intrusion. Winds can induce circulation and promote mixing within the water column, particularly in the surface layer. The impact of wind can be divided into two distinct components: local wind and remote wind (Gong et al., 2022; Wong and Lu, 1994). Local wind exerts a direct influence on the water surface of the estuary, thereby modifying the mixing and circulation dynamics within the estuary, which in turn affects the extent of saltwater intrusion. Specifically, local wind stress can facilitate the advancement of saltwater into estuaries when directed upstream, whereas down-estuary winds can reduce the extent of saltwater intrusion (Perales-Valdivia et al., 2018). Conversely, remote winds modulate the water elevation and salinity at the estuary mouth, thereby exerting an indirect effect on saltwater intrusion. In addition, climate change is also recognized as one of the primary factors that will influence estuary saltwater intrusion in the future, since the global warming is causing sea level to rise significantly (Wei et al., 2015).

The modern Yellow River (YR) Delta is located in the southwestern region of the semi-enclosed Bohai Sea and plays a crucial role in flood regulation and economic development (Zhang et al., 2016). It also serves as a vital habitat for numerous precious plant species such as wild soybean, and endangered avian populations such as Black-faced Spoonbill and Mute Swan (Zhang et al., 2016). Xia et al. (2021) indicated that the Yellow River Delta is encountering severe saline intrusion in its coastal aquifer, which poses great threats to water quality and the ecological integrity of the wetland area. However, there are very few studies about the saltwater intrusion within the river channel of Yellow River Estuary (YRE). Most of salt-related studies about the estuary have focused on the behaviour of low-salinity water in the offshore area of the estuary. Given the increasing concerns on maintaining species diversity and safeguarding water resources, this issue has become critical from the perspective of coastal management and conservation.

Moreover, the Yellow River Delta is characterized by unique hydrodynamic features that differentiate it from other major deltas. The evolution of the Yellow River has established a high-energy fluvial system within the estuary, where seasonal floods drive significant sediment delivery to the Bohai Sea (Lin et al., 2025). Both field investigations and numerical modelling have identified the existence of an M_2 amphidromic point near the mouth of the Yellow River, a geographical location with zero tidal amplitude for M_2 constituent (Huang et al., 2015; Ji et al., 2020). This reduced M_2 amplitude leads to a micro tidal range and a diurnal tidal regime dominated by K_1 and O_1 within the Yellow River estuary. Aside from precipitation patterns related to monsoon and other atmospheric processes in the upper reaches (Zhao et al., 2024), the river's runoff is also largely modulated by human activities, particularly through the Water-Sediment Regulation Scheme (WSRS) implemented upstream. This scheme releases up to 30% of the annual runoff into the Bohai sea within a short period of two weeks, thereby substantially altering the natural seasonal variability of river discharge and the water-sediment processes in the lower reaches (Ji et al., 2018; Jia and Yi, 2023; Lin et al., 2024). As river discharge and tidal forcing are recognized as the primary controls of estuarine saltwater intrusion, these dynamic characteristics are likely to create a distinct pattern of saltwater intrusion in the YRE compared to other middle-latitude estuaries, such as the widely-studied Changjiang Estuary (Qiu et al., 2012) and Hudson River Estuary (Ralston et al., 2019). Therefore, investigating saltwater intrusion within the YRE holds great scientific significance.

To date, several observational and numerical studies have examined the salinity distribution in the Yellow River Estuary, although most have focused on the offshore areas of the estuary. Principally, the distribution of low-salinity water in the estuary corresponding to the Yellow River plume exhibits clear seasonal variation in response to seasonal variations in the wind field and river discharge (Gai et al., 2025; Qin et al., 2023; Wang et al., 2008). In summer, prevailing southeasterly winds facilitate the offshore movement of the plume, which typically extends northeastward into the central Bohai Sea. In contrast, northerly winds during winter drive the low-salinity water into Laizhou Bay (Qin et al., 2023). The range of low-salinity area is also closely linked to the river discharge, growing larger and shifting southward as discharge increases. Consequently, the river plume is most pronounced in summer, when river discharge reaches its peak (Gai et al., 2025; Wang et al., 2008). Additionally, the distribution of low-salinity water is affected by northward tide-induced residual currents offshore of the Yellow River mouth, which can cause the upstream extension of the plume, particularly under low runoff conditions in spring (Yu et al., 2021). However, little attention has been given to the salinity structure within the Yellow River channel.

This manuscript serves two primary purposes. First, it seeks to document, for the first time the along-estuary salinity structure in the YRE, along with its temporal variations. Second, it presents observational evidence, albeit limited, regarding the short-term and seasonal variability of salinity intrusion associated with tidal fluctuations and wind conditions. It is anticipated that the findings reported herein will contribute to the management and conservation initiatives of the Yellow River Delta coastal system. The remainder of the paper is organized as follows: Section 2 provides a brief description of the in-situ hydrological data collection methods. Section 3 presents the results. The discussion and conclusions are provided in Section 4 and Section 5, respectively.

2. Field observations

To examine the seasonal variations in saltwater intrusion at the Yellow River Estuary (YRE, Fig. 1a and b), a series of observations utilizing mooring instruments and shipboard surveys within the river channel were conducted during the spring and autumn of 2023. In the spring, an anchor-based tide gauge and a buoy mounted with a conductivity–temperature–depth profiler (CTD) were deployed 0.9 km upstream of the river entrance (indicated by the red dot in Fig. 1c). The two instruments facilitated the collection of surface salinity and water depth data at 10-min intervals from May 10 to May 27, encompassing a complete spring-neap tidal cycle. Additionally, along-channel shipboard surveys were performed on May 11 (spring tide) and May 19 (neap tide). Each survey followed an axial path with an along-channel resolution of about 200 m (marked by black and blue dots in Fig. 1c) and required roughly 0.5 h. Salinity casts with a multi-parameter water quality

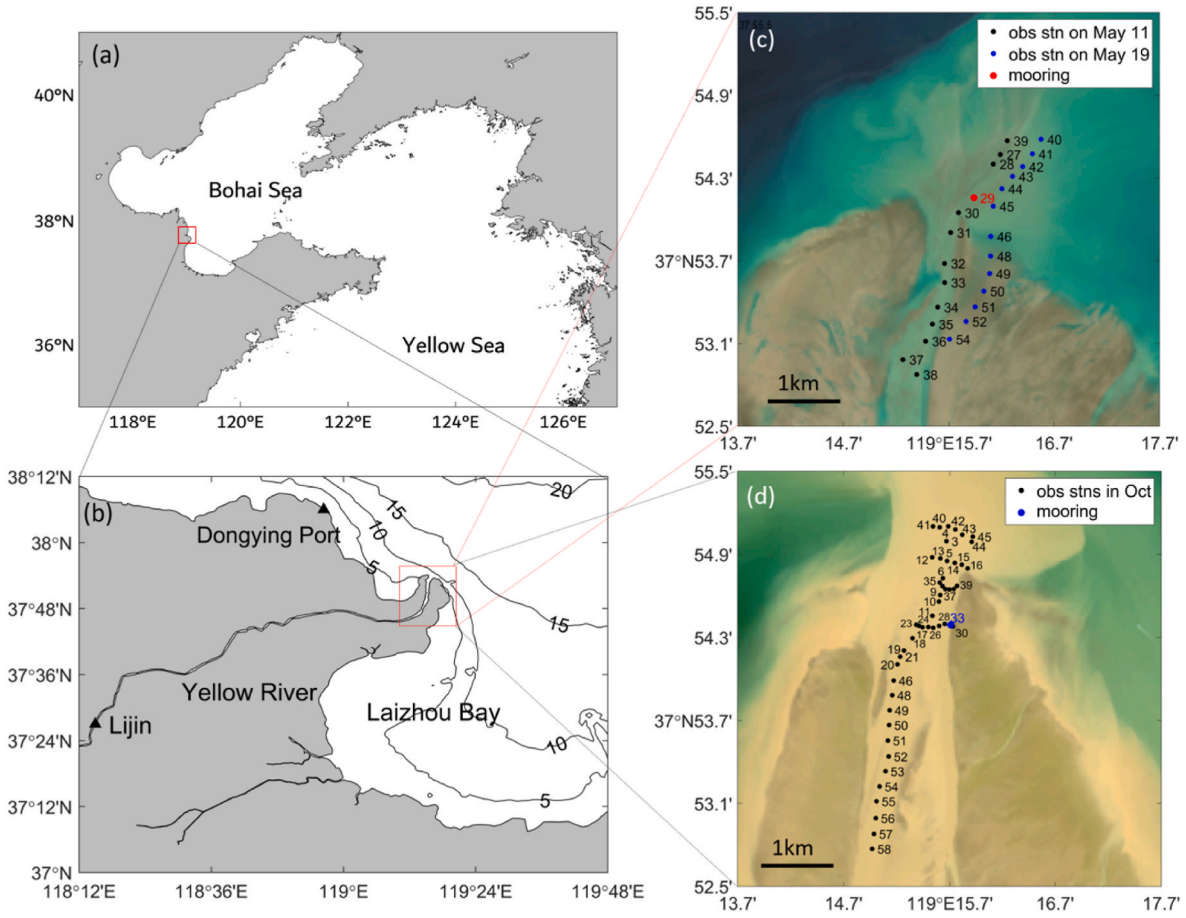

Fig. 1. (a) Geographical location of the Yellow River Estuary within the Bohai Sea and (b) the specific area of study. River estuary topography and the locations of observational stations are depicted for (c) May and (d) October 2023. In panel (c), black dots represent sampling stations on May 11, and blue dots denote those on May 19; while the red dot marks the position of the mooring instruments. In panel (d), black dots denote the sampling stations, while the blue dot represents the location of mooring measurement. (For interpretation of the references to colour in this figure legend, the reader is referred to the Web version of this article.)

detector were taken at these stations at 3-h intervals to capture intra-tidal variations of saltwater intrusion.

In the autumn, two sets of CTD and Acoustic Doppler Current Profiler (ADCP) instruments were deployed 1.5 km upstream of the river entrance (indicated by blue dot in Fig. 1d) from October 15 to October 30, 2023. One set was mounted on a buoy to collect surface current and salinity data, while the other was affixed to a pole embedded in the bottom mudflat (approximately 50 cm above the seabed) to record bottom current, water depth and salinity data. Furthermore, one longitudinal section and four lateral sections (marked by black dots in Fig. 1d) were selected for shipboard surveys using the same instrument and configurations as those deployed in May. The locations of the sampling stations were redesigned due to significant alterations in the river estuary's topography resulting from the continuous erosion and siltation from May to October 2023. Shipboard surveys along these stations were conducted on three occasions: on October 15 (neap tide) with strong northeasterly winds, October 22 (spring tide) and 30 (neap tide) with weak southerly winds. The surveys on October 22 and 30 had provided comprehensive records of the upstream movement of saline water into the channel under both spring and neap tidal conditions. Additionally, records from October 15 were compared with those from October 30 to basically illustrate the effect of wind direction on salinity distribution within the YRE.

In addition to the in-situ hydrographic data, various auxiliary datasets were collected during the survey period, which included the Yellow River discharge, as well as wind and tidal levels at Dongying Port, a site representative for tidal elevations outside the river estuary. Daily discharge data for the Yellow River were obtained from the Lijin Station, located approximately 100 km upstream from the river estuary (refer to Fig. 1b for its location). According to Wang et al. (2011), this distance between Lijin Station and the Yellow River mouth will cause a time lag of ~10 h between the record of river discharge and its arrival time. Hourly wind data over YRE were provided by Yantai Institute of Coastal Zone Research. Additionally, hourly tidal levels at Dongying Port were sourced from the National Ocean Information Center (available at https://mds.nmdis.org.cn/pages/tidalCurrent.html). All auxiliary data collected during the observational periods in spring and autumn are illustrated in Figs. 2 and 4.

Real-time coastline data for May and October 2023 were derived from satellite imagery. Remote sensing images of the Yellow River estuary were acquired from Landsat 8 (available at https://earthexplorer.usgs. gov) and subsequently processed using Arcgis 10.8, which facilitated the registration of Landsat images to geographic coordinates, thereby enabling the extraction of the latitudinal and longitudinal positions of the shoreline. The location of the Yellow River entrance (designated as Stations No. 39 and 40 in Fig. 1c; No. 4 Station in Fig. 1d) was determined by the Yellow River Conservancy Commission of the Ministry of Water Resources and evolved constantly in response to real-time changes in the depth within the river channel.

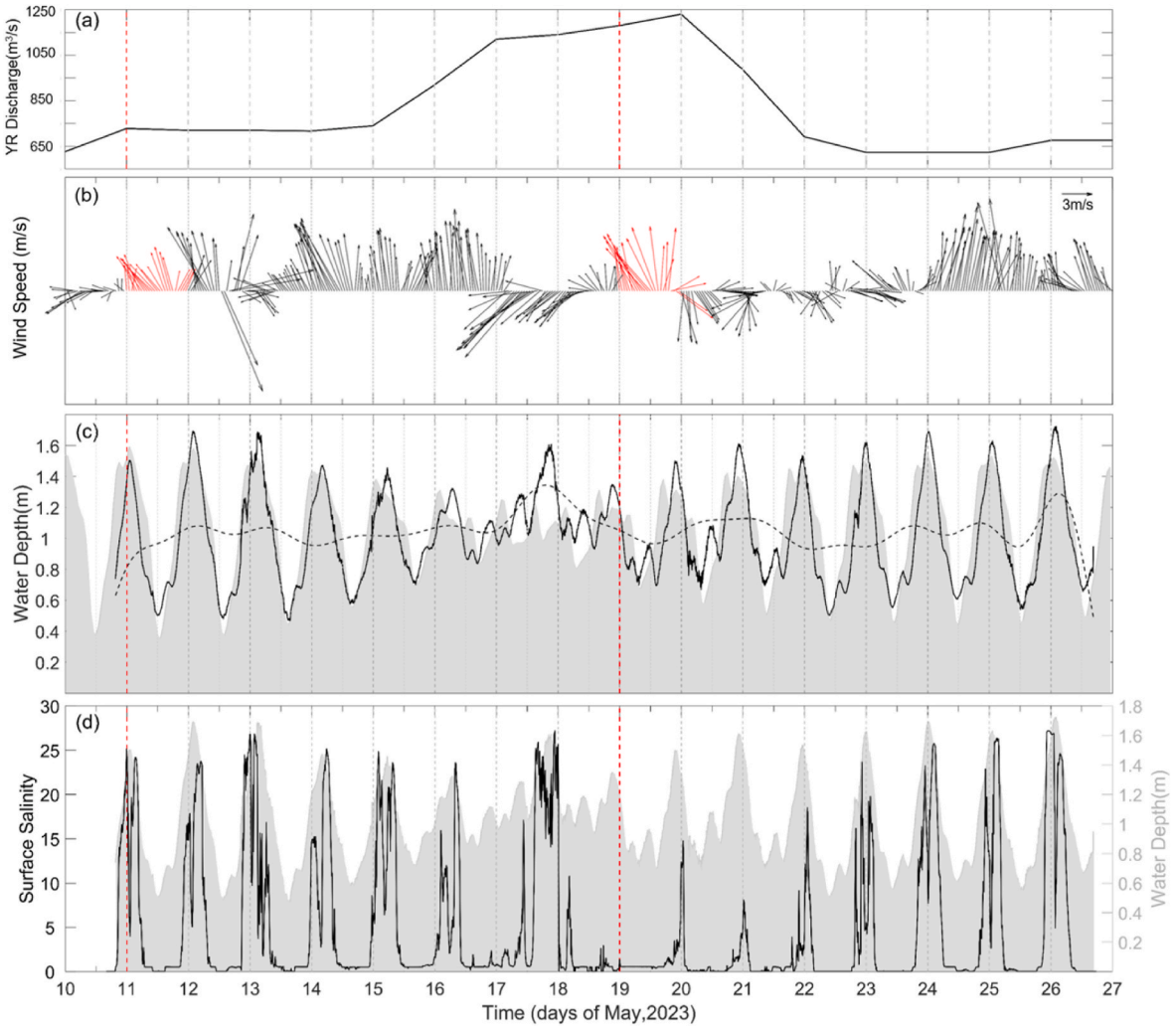

Fig. 2. Time series of (a) Yellow River discharge and (b) wind conditions near the river estuary, together with (c) observed water depth (with solid line representing observed data and dashed line indicating low-pass filtered values of observed data; the grey area denotes water depth at Dongying port) and (d) observed surface salinity (with solid line for the observed salinity and the grey area for observed water depth) at Station No. 29 in the river channel during the period from May 10 to May 27, 2023. The red dashed lines in panels (a), (c) and (d) indicate the commencement dates of shipboard surveys, while the red arrows in panel (b) denote the wind data collected during these surveys. (For interpretation of the references to colour in this figure legend, the reader is referred to the Web version of this article.)

3. Result

3.1. Spring survey

3.1.1. Temporal variation of saltwater intrusion in the YR

During the survey period from May 10 to May 27, 2023, the Yellow River discharge fluctuated between 550 m^3/s and 1250 m^3/s (Fig. 2a). The prevailing wind near the river estuary was predominantly southerly with an average wind speed of 7.4 m/s, while significant northeasterly and northerly wind events were recorded on May 17 and 20 (Fig. 2b).

The measured water depth at No. 29 station within the river channel varied almost synchronized with the tidal level at Dongying Port (Fig. 2c), with a time lag of about 0.5 h. Tide at the Dongying Port is predominantly diurnal and displays a distinct fortnightly signal. A harmonic analysis using Matlab toolkit "s_tide" (Pan et al., 2018) was applied to the water level at Dongying Port, with the amplitudes and phases of the main tidal constituents given in Table 1. The tidal form factor, which is the ratio between diurnal (K_1+O_1) and semidiurnal (M_2+S_2) constituents, is 3.24, characteristic of a diurnal tide. The tidal ranges recorded at Dongying Port were 1.2 m during spring tides (on May 12 and 25) and 0.25 m during neap tides (on May 18), with semidiurnal tides becoming more prominent during neap conditions.

Table 1
Tidal components for the tidal level at the Dongying port. Amplitude (A) and phase (G) are shown.

Tidal constituents	Period (h)	A (cm)	G (deg.)
M_2	12.42	10.3	99.0
S_2	12.00	5.1	152.4
K_1	23.93	26.4	148.4
O_1	25.82	23.5	104.5

The water depth measured within the river channel retained most of the tidal features observed at the Dongying Port, including diurnal and fortnightly variations. However, the water level deviated substantially from the tidal level at Dongying Port on May 17. A low-pass filter with a cutoff frequency of 25 h was applied to emphasize the sub-tidal oscillations present within the estuary (indicated by the dashed line in Fig. 2c). Minor sub-tidal water level fluctuations of less than 0.1 m were observed throughout the monitoring period, except for May 17, when an increase of 0.3 m was recorded, resulting in a substantially elevated water level. Consequently, we hypothesize that the elevated water level was a result of the intense northeasterly winds, which facilitated the influx of substantial amounts of seawater into the river channel. Besides,

we observed that the high tide in the river channel consistently occurred during the night time hours in May.

Despite the evident diurnal pattern of water levels in the river channel, the measured surface salinity in the river channel exhibited a semidiurnal variation for most of the study period (Fig. 2d). This salinity demonstrated two prominent peaks characterized by uneven amplitudes within a 24-h cycle. Notably, the intervals between the two peaks of surface salinity were brief, with the declines between two peaks occurring concurrently with the peaks in water level. The procedure by which surface salinity alterations occur is delineated as follows. Surface salinity began to rise approximately 3 h after the lowest tide, reaching a peak value before declining, only to rise again to a second peak shortly after the highest tide. Subsequently, surface salinity decreased rapidly as the water levels began to recede. The duration of low salinity (salinity <2) was observed to be longer than that of high salinity (salinity >5) within a single day. Similar with water levels, the peak surface salinity in the river channel exhibited a fortnightly variation, particularly evident in the increasing trend from May 19 (neap tide) to May 26 (spring tide). The notably high salinity recorded on May 17 was likely due to the strong northeasterly winds that transported significant volumes of sea water from outside into the river channel. There was also a phenomenon where a small amount of seawater intruded into the river on May 18 and 19.

3.1.2. *Vertical distribution of salinity in the YR*

Salinity profiles along the river channel were assessed on May 11 and May 19 to illustrate both intra-tidal and fortnightly variations in saltwater intrusion within the YR (Fig. 3). Note that the saltwater intrusion length was determined here with the location of the bottom 2-isohaline. On May 11 (spring tide), the tide exhibited a diurnal pattern (grey line in Fig. 3a). Approximately 1 h before the highest tide (~00:00), the water elevation at Station No. 29 reached 1.4 m, with saltwater intruding approximately 3.0 km from the river estuary into the channel (Fig. 3b). The salinity recorded at Station No. 29 was about 26 throughout the entire vertical column, while the bottom salinity at Station No. 37 was about 8. A pronounced stratification was observed, quantified at approximately 10 m^{-1}, indicating that the saltwater predominantly intruded through the bottom layer. Additionally, a pronounced upright salinity front was observed between Stations No. 36 and No. 37 in the bottom layer, alongside a pronounced pitched front between Stations No. 31 and No. 29 in the surface layer. At about 06:00, during the mid-ebb tide (Fig. 3c), the saltwater had receded compared to its position at 00:00. The bottom salinity at Station No. 39 was about 24, while the salinity at Station No. 29 was recorded at 2 at the surface and 14 at the bottom. By around 09:00, saltwater had flowed out to Station No. 27 (Fig. 3d). At about 12:00, during lowest tide, salinity levels in the entire river channel approached zero (Fig. 3e). Throughout the ebb tide (from 00:00 to 12:00), as the water elevation decreased (Fig. 3a), saltwater was expelled from the river channel, resulting in a reduction in salinity. The maximum observed intrusion distance during the spring tide was about 3.0 km upstream from the river estuary.

On May 19 (neap tide), the tide shifted to a semidiurnal pattern,

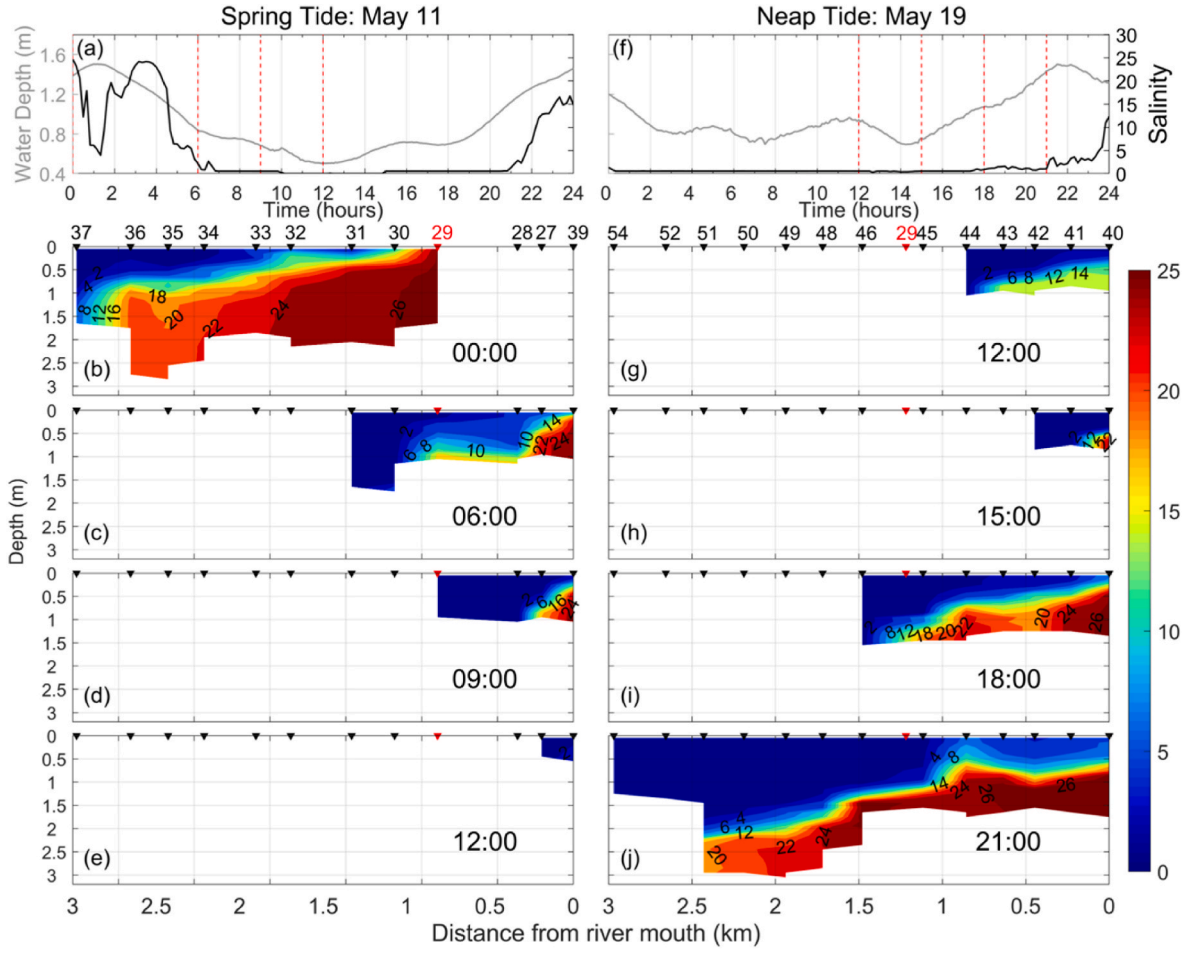

Fig. 3. Water depth (grey line) and surface salinity (black line) at the mooring station, alongside the longitudinal salinity distribution within the river channel at different stages of the tidal cycle during (a–e) spring tide and (f–j) neap tide. The x-axis in panels (b)–(e) and (g)–(j) represents the distance from the river estuary during the survey and the red triangle marks the location of the mooring instruments. The red dashed lines in panels (a) and (f) signify the commencement of each survey. (For interpretation of the references to colour in this figure legend, the reader is referred to the Web version of this article.)

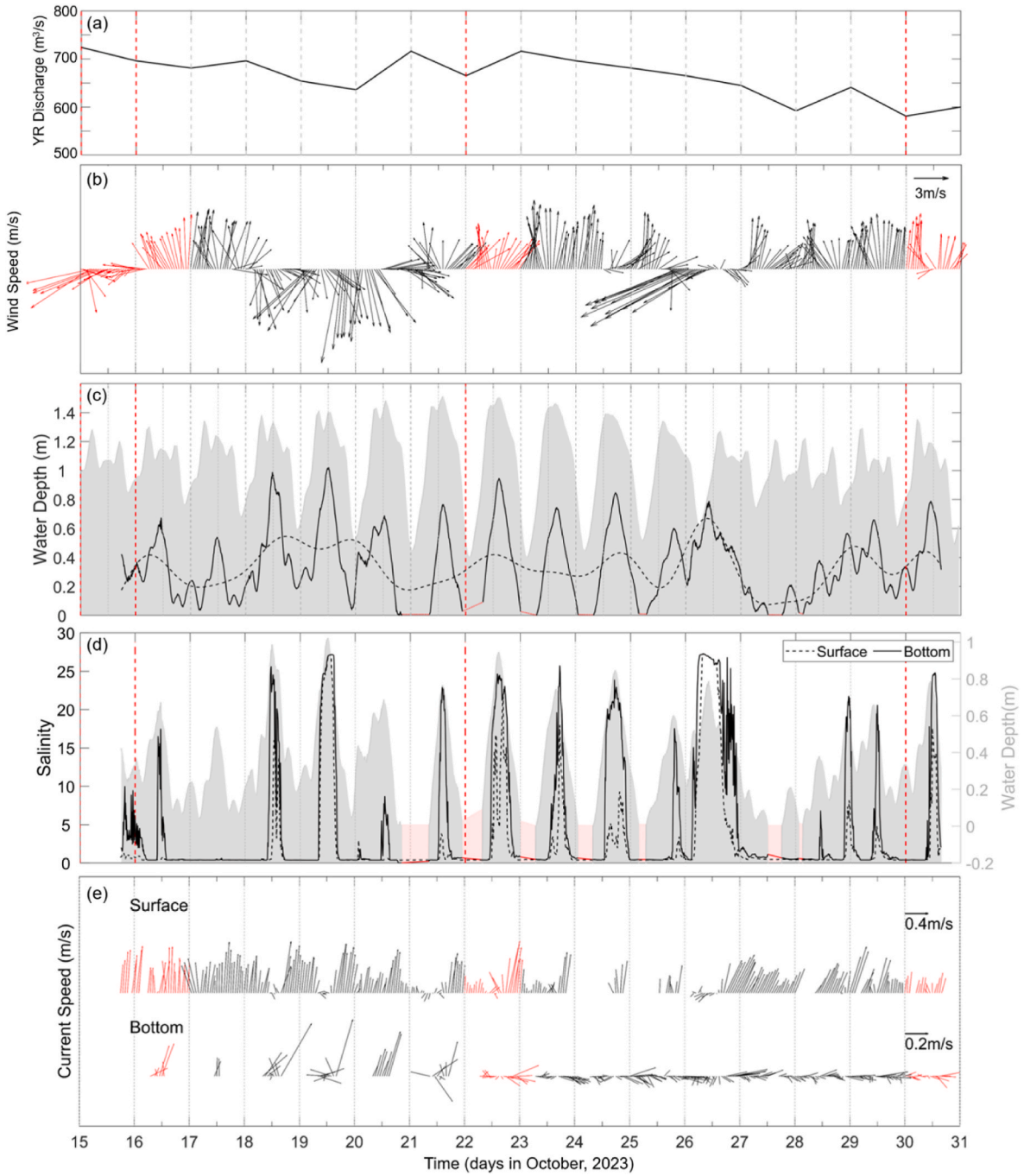

Fig. 4. Time series of (a) Yellow River discharge and (b) wind conditions near the river estuary, together with (c) observed water depth (solid line for observed data and dashed line for low-pass filtered depth; missing data represented by a dotted blue line; the grey area denotes tidal elevation at Dongying Port), (d) observed salinity (dashed line for the surface salinity and solid line for bottom salinity; missing data is represented by a dotted blue line; the grey area represents observed water depth, with missing data covered by blue areas) as well as (e) observed surface and bottom currents at Station No. 33 in the river channel from October 15 to 30, 2023. The red dashed lines in panels (a), (c) and (d) mark the initiation dates of the shipboard surveys, while the red arrows in (b) and (e) denote the winds and currents recorded during each survey. (For interpretation of the references to colour in this figure legend, the reader is referred to the Web version of this article.)

characterized by two floods and two ebbs within a single day (grey line in Fig. 3f). At the initial small peak of water elevation at Station No. 29 (~1 m, at 12:00), the salinity within the river channel was approximately 14 at the bottom, with an intrusion distance measured about 0.8 km (Fig. 3g). At the lowest tide (~15:00), salinity levels within the channel were minimal (Fig. 3h). By the middle time of flood (approximately 18:00), the salinity at the river estuary reached about 26 at the bottom, with the intrusion distance extending to approximately 1.5 km (Fig. 3i). At this time, a strong upright salinity front was observed in the inner section of bottom channel, while a pronounced pitched salinity front was noted in the outer section of surface channel. During the second peak of water elevation at Station No. 29, which reached approximately 1.4 m at 21:00, the observed intrusion distance was at its maximum, measuring around 2.5 km, with the highest recorded salinity at the bottom being approximately 26 (Fig. 3j). The stratification during this period was notably pronounced, quantified at approximately 13 m^{-1}. Throughout the flood tide (from 15:00 to 21:00), an increase in water elevation was accompanied by a corresponding rise in salinity

within the river channel (Fig. 3f). It is noteworthy that the intrusion distance during the neap tide was smaller, measuring 2.5 km, compared to 3.0 km during the spring tide.

3.2. Autumn survey

3.2.1. Temporal variation of saltwater intrusion in the YR

During the observation period from October 15 to 30, 2023, the Yellow River discharge remained relatively constant, averaging 650 m^3/s (Fig. 4a). Winds near the river estuary predominantly came from the south, with an average wind speed of 5.6 m/s, however, notable events of strong northeasterly or northerly winds were recorded on October 15, 18–19, and 26 (Fig. 4b).

Similar with the conditions observed in May, the tidal pattern at Dongying Port exhibited diurnal and fortnightly characteristics (grey area in Fig. 4c). The tidal range was greatest on October 22, measuring 1.1 m during spring tide, and smallest on October 15 and 29, at 0.3 m during neap tide. Additionally, a semidiurnal signal was observed during neap tide. Tide within the river channel mirrored that of Dongying Port, displaying a diurnal signal during the spring tide and a semidiurnal signal during the neap tide (solid line in Fig. 4c). However, the fortnightly signal in the water levels within the channel was not pronounced. Notably, the tidal ranges on October 18, 19, and 26 were unexpectedly significant, coinciding with the occurrence of northerly wind events. Furthermore, we noted that, in contrast to May, when high tides occurred predominantly at night, high tides in October were observed during the daytime. Specifically, high tide was recorded around 12:00 on October 16, with the timing progressively advancing to approximately 18:00 on October 25. Following this adjustment, the timing reverted to 10:00 on October 26, subsequently advancing again to about 12:00 on October 30. It is important to highlight that the distinct set-down of water level caused the bottom instruments at Station No. 33 to become exposed during the ebb tides from October 21 to 25 (a period of zero water level), leading to data gaps in the measured salinity and velocity.

The surface salinity recorded in October within the river channel exhibited a semidiurnal variation, similar to the patterns observed in May, except for October 19 and 26 (dashed line in Fig. 4d). In contrast, the bottom salinity demonstrated a diurnal variation (solid line in Fig. 4d), with peaks in bottom salinity and water level occurring simultaneously. Moreover, the bottom salinity generally exceeded surface salinity on most days, except for October 19 and 26, when the two measurements were nearly identical. The fortnightly variation in salinity is not pronounced. During the spring tide on October 22, salinity levels were elevated (~24), yet they were even higher on October 18, 19 and 26 (exceeding 25), coinciding with periods of strong northerly winds. We hypothesize that these strong northerly winds facilitated the influx of seawater into the river channel thereby increasing salinity and promoting vertical mixing, which resulted in a more vertically homogeneous salinity profile. A similar phenomenon observed in May was also noted in October, specifically the absence or minimal occurrence of saltwater intrusion on October 20, and 27. Notably, strong northerly winds were present prior to these three days. The reason for the absence of saltwater intrusion on the second day following strong northerly winds warrant further investigation, particularly in the context of sustained high-water levels.

The surface current at Station No. 33 primarily demonstrated an outflow pattern, except for high tide events, during which the current transitioned to an inward flow along the river channel (Fig. 4e). The velocity of the outflow current was approximately 0.83 m/s, whereas the inward current speed was only about 0.15 m/s. In contrast, the bottom current displayed a relatively chaotic behaviour, predominantly flowing westward during the first half of the day and shifting to an eastward direction in the latter half on most days.

3.2.2. Vertical distribution of salinity in the YR

We conducted sectional surveys along the river channel on October 15, 22, and 30. On October 15 (neap tide), the survey commenced at approximately 07:30, during a low tide (not recorded by the mooring instrument but observed on-site). At this time, most of the river channel was occupied by freshwater, with saltwater beginning to intrude upstream from the bottom layer (Fig. 5a). Two hours later, around 09:00, the saltwater had advanced about 1 km from the river estuary (Fig. 5b). Following this, a strong northeasterly wind commenced. By approximately 12:00, the 2-isohaline had progressed an additional 1 km (Fig. 5c). In comparison to the conditions prior to the onset of the strong wind, the salinity profile became vertically homogeneous following the wind event. By around 14:00, the saltwater had receded from the river channel (Fig. 5d). Throughout this observation period, the maximum distance of saltwater intrusion extended approximately 2 km from the river estuary, with the maximum salinity in the bottom layer of the river channel recorded at 26. The zonal section survey indicated that salinity was vertically stratified at around 10:00 (Fig. 7a), suggesting that the high-salinity water intruded from the bottom. Furthermore, the saltwater did not enter from any specific side but rather intruded synchronously along the entire channel. Following a strong northeasterly wind, the salinity became vertically homogeneous by approximately 12:30 (Fig. 7b).

On October 22, during a spring tide, surveys were conducted at 08:00, 10:20, 12:00, and 14:00, effectively covering the flood period from the lowest tide to the highest tide (Fig. 6a). The intrusion distance increased from 500 m to 4.5 km (Fig. 5e–h), with the highest salinity recorded at 26 in the bottom layer. During this survey, four zonal sections were analysed at different tidal times. The results consistently indicated that the isohalines were horizontal (Fig. 7c–f), suggesting that the high salinity water intruded from the bottom on both sides of the river channel.

To further investigate the saltwater intrusion during neap tide under southerly winds, we conducted another survey on October 30, from 08:00 to 14:00, encompassing both flood and ebb periods (Fig. 6b). The maximum intrusion distance reached approximately 2.5 km, occurring around 12:00 (Fig. 5k). In comparison to the intrusion observed during spring tide under southerly winds on October 22, the intrusion was less pronounced measuring about 2 km shorter.

However, it is challenging to compare the intrusion patterns under both northeasterly and southerly winds during neap tide based on the sectional distribution, as the water depth in the river channel was not recorded on October 15, rendering the tidal cycle especially the timing of high tide unknown.

3.3. Tide dynamics and its influence on saltwater intrusion within YRE

The analysis of observational data indicates that tidal characteristic inside the YR channel exhibit similarities to those observed at Dongying Port, situated approximately 30.8 km north of the YR mouth. The tidal range recorded at Dongying Port (dashed line in Fig. 8a) revealed that the dates of May 12 and May 25 aligned with spring tides, corresponding to the 23rd and 7th days of the lunar calendar, respectively. Conversely, the date of May 18 coincided with a neap tide, corresponding to the 29th day of the lunar month. This periodicity contrasts with the widely accepted understanding that spring tides generally occur during the new and full moon phases, whereas neap tides are associated with the first and last quarter moon phases. Actually, this spring-neap cycle synchronized with the Moon phases is typically applicable for semidiurnal tides, yet it is not pertinent to the case within Yellow River Estuary, where semidiurnal oscillation is weak. Indeed, the dominant K_1 and O_1 constituents within YR Estuary are governed by the variation in lunar declination, as described by Pugh (1987). Diurnal spring tides occur when the Moon reaches its maximum northern or southern declination, while the corresponding neap tides take place when the Moon is positioned over the Earth's equator. This change in lunar declination reflects

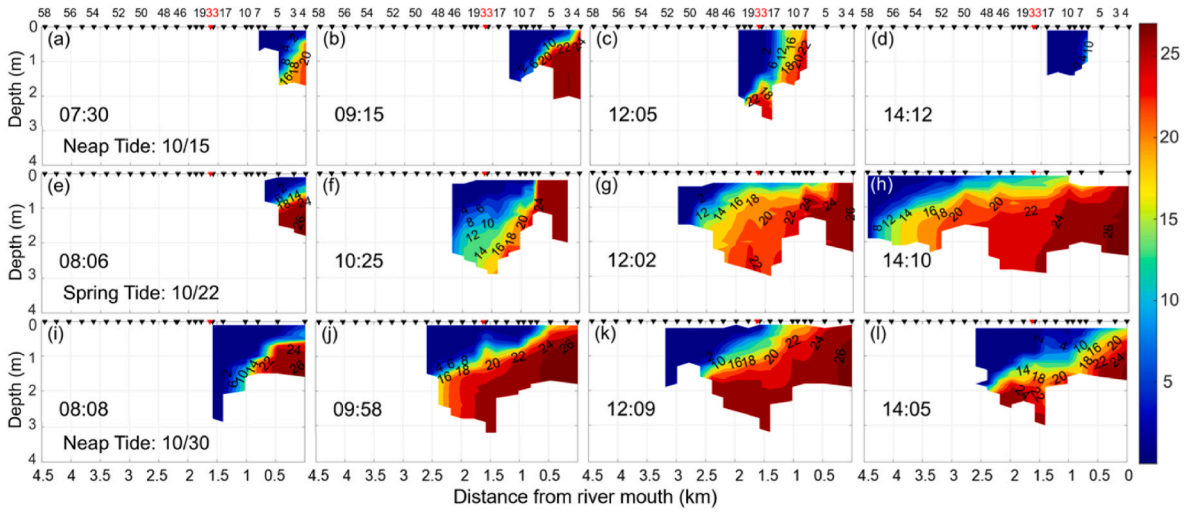

Fig. 5. Vertical distribution of salinity along the longitudinal section of the river channel at various tidal times on October 15 (upper panel, characterized by northeasterly winds), October 22 (middle panel, influenced by southerly winds), and October 30 (lower panel, also under southerly winds). The columns represent surveys conducted at approximately 08:00, 10:00, 12:00, and 14:00, respectively. The x-axis represents the distance from the river estuary for this survey and the red triangle marks the along-stream position of the mooring instruments. (For interpretation of the references to colour in this figure legend, the reader is referred to the Web version of this article.)

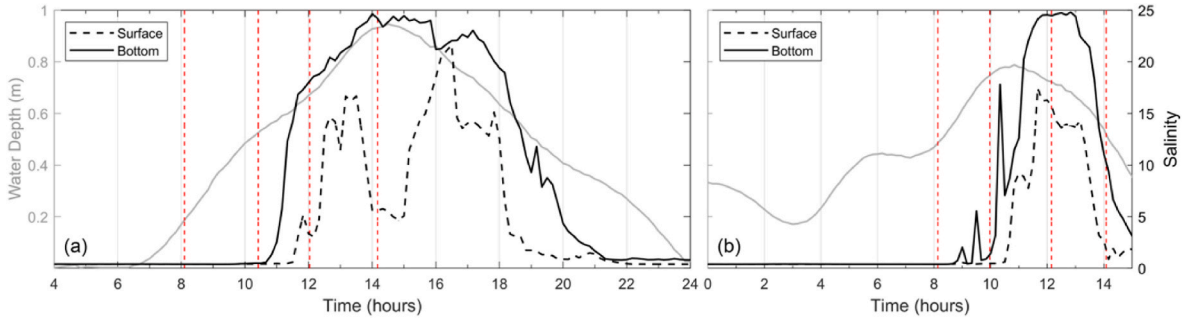

Fig. 6. Observed water depth (grey line) as well as the surface (dashed line) and bottom salinity (solid line) measured at the mooring station on (a) October 22 and (b) October 30. Red dashed lines indicate the timing of each survey shown in Fig. 5. (For interpretation of the references to colour in this figure legend, the reader is referred to the Web version of this article.)

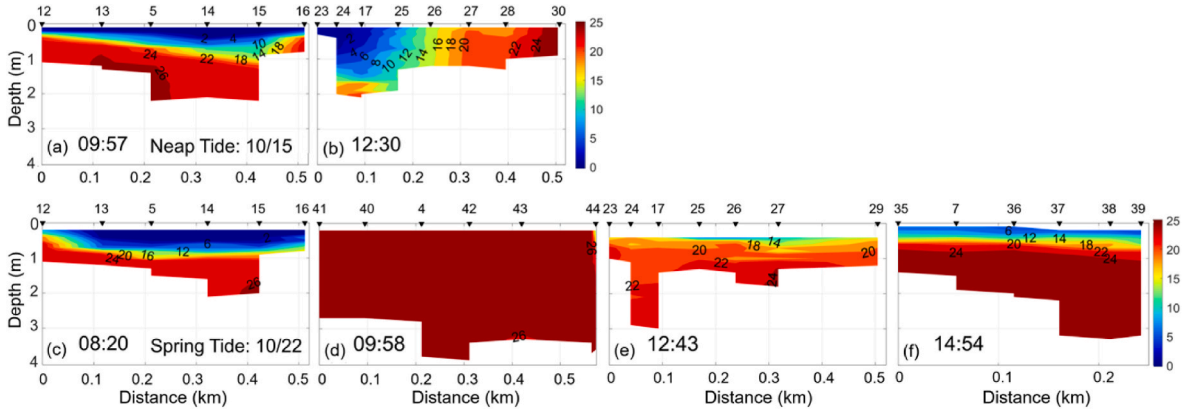

Fig. 7. Vertical distribution of salinity on the sections across the river channel at different tidal times on October 15 (upper panel) and October 22 (lower panel).

the movement of the Moon in its 27.32-day orbital cycle around the Earth, commonly referred to as a tropical month in astronomical terms. Our calculations of lunar declination during the survey period (grey area in Fig. 8) also reveal that the dates of the maximum and minimum tidal ranges align with the arrival of the maximum Moon declination (May 10 and May 23) and the date when the Moon crosses the Equator (May 16), respectively, with an average lag of 2 days. During the spring tides, the tidal pattern is predominantly diurnal, whereas during the neap tides, it becomes semidiurnal. This semidiurnal pattern occurs because the diurnal tidal constituents (K_1 and O_1) diminish sharply during neap tides, enabling the semidiurnal M_2 constituent to dominate tidal oscillations. It is worth noting that such tropical tidal cycles are not unique to

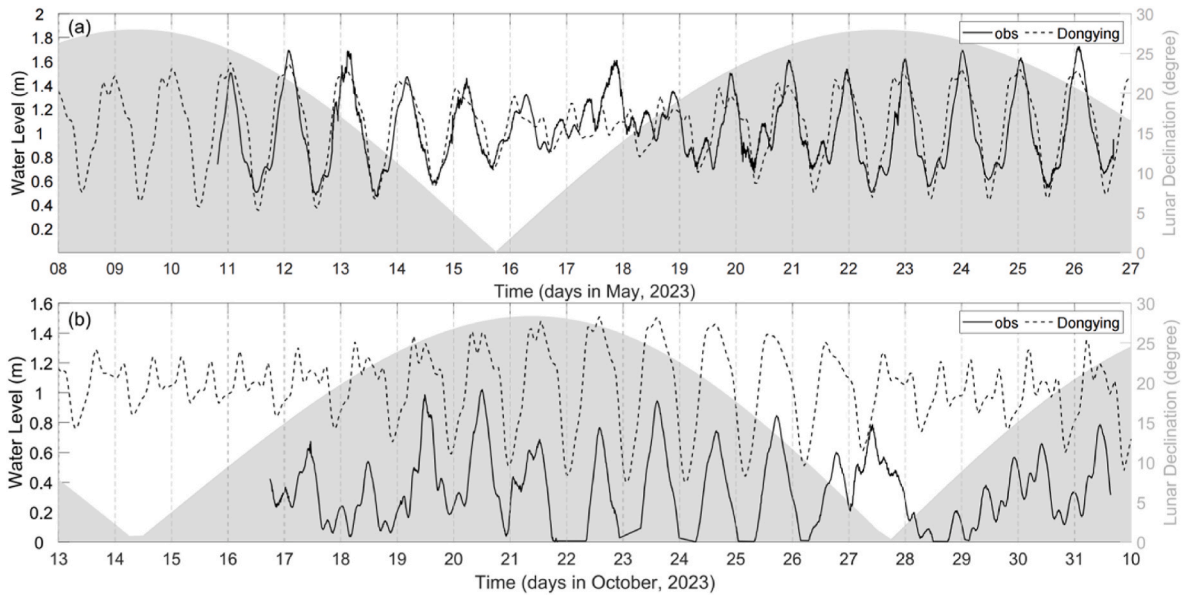

Fig. 8. Time series of water elevation at Dongying Port (dashed line) and the measurements taken within the YR channel (solid line), alongside the lunar declination (grey area) in (a) May and (b) October 2023.

this region; similar patterns have been observed in other river estuaries around the world, such as the Mobile Bay Estuary (Kim and Park, 2012) and the Amazon Estuary (Gallo and Vinzon, 2005). However, few studies have documented this tropical cycle within the YRE, and this research provides a more comprehensive understanding of tidal dynamic in this region.

Furthermore, a comparative analysis of water elevation in the river channel during May and October 2023 revealed that high tides during spring tides consistently occurred around midnight in May, while they were observed around noon in October during our survey (Fig. 8). This discrepancy can be attributed to the dominance of the K_1 tidal constituent near the YR estuary, which has a tidal amplitude of approximately 26.4 cm as determined through the harmonic analysis of observed water depths during the May survey. This amplitude exceeds that of the O_1 (23.5 cm), M_2 (10.3 cm) and S_2 (5.1 cm) constituents. The K_1 tidal cycle spans 23.93 h, which is slightly less than the 24-h cycle of a typical day. From May to October 2023, the timing of high tides can advance by approximately 12 h, calculated as follows: (24-23.93) hours/day*170 days.

The tidal dynamics within the river channel exert a significant impact on the intrusion of saltwater. Observational data reveal that surface salinity exhibits a semidiurnal variation (Figs. 2d–4d), whereas bottom salinity demonstrates a diurnal variation trend (Fig. 4d). When the water elevation in the YR channel rises to approximately 0.9 m in May and 0.5 m in October, both surface and bottom salinity levels begin to increase. Prior to reaching the peak tide, surface salinity decreases while the bottom salinity continues to rise. At the peak tide, bottom salinity attains its maximum value, while surface salinity drops to its minimum. Subsequently, surface salinity increases to a secondary peak, whereas bottom salinity declines. Ultimately, both surface and bottom salinity decrease in conjunction with the water elevation.

To further examine the variation in salinity periodicity between the surface and bottom layers, we conducted an analysis of the fluctuations in currents and salinity at both the surface and bottom moorings on October 22. Since data were missing at low tide on some dates, only the current series from October 20 to 22 were subjected to a quasi-harmonic analysis, in which four principal tidal constituents O_1, K_1, M_2, and S_2 were included. The amplitudes and phases of each constituent were derived using the Matlab toolkit 's_tide' (Pan et al., 2018), and were then used to calculate the tidal currents for October 22.

The observed surface current was predominantly directed outward throughout most of the day, exhibiting a weaker velocity prior to 15:00 and a stronger velocity thereafter (Fig. 9a). The surface tidal current displayed a diurnal pattern, characterized by an inward flow before 15:00 and an outward flow following this time (Fig. 9a). This variation suggested that the inward tidal current impeded the outward fluvial flow, resulting weak outward surface current. Conversely, when the tidal current transitioned to an outward direction, it facilitated the outward fluvial flow, thereby enhancing the strength of the outward surface current. During the late flood tide (from 11:00 to 14:00), the robust inward tidal current promoted the upstream transport of saline water towards the mooring, resulting in an increase in salinity levels to approximately 15. Approaching the high tide at 13:30, the slackening flood current weakened the upstream transport of saltwater. Concurrently, a significant volume of freshwater was discharged outward from the surface, resulting in a rapid dilution of surface salinity, which decreased to about 5. Shortly after high tide, as the ebb tide commenced, salinity rose again to approximately 20 by 16:00, before gradually declining to zero by 18:00. This peak in salinity during the early ebb may be attributed to the saline water that had been introduced into the river channel during the preceding flood tide, which was subsequently advected downstream by the ebb current and passed through the mooring.

Although the span of the bottom currents series was insufficient for harmonic analysis, the observed bottom currents on October 22 demonstrated distinct diurnal variation with the flooding and ebbing periods. The flow direction was predominantly westward throughout the flood period, which facilitated the ingress of seawater into the river channel, resulting in an increase in salinity concurrently with the rising water level. During the ebb, significant eastward currents persisted, leading to the efflux of seawater from the river channel, which caused a synchronous decrease in both salinity and water level. The currents and salinity in the bottom layer were primarily influenced by the tidal currents.

In addition to the intra-tidal fluctuations in salinity driven by tidal forces, the salinity in the river channel exhibited fortnightly and seasonal variations. Observational data indicated that the peak salinity level within the channel was higher during spring tides compared to neap tides. Furthermore, the extent of saltwater intrusion was also greater during spring tides, measuring 3.0 km in May and 4.5 km in October, as opposed to 2.5 km in both May and October during neap tides. The maximal saltwater intrusion was recorded at midnight during

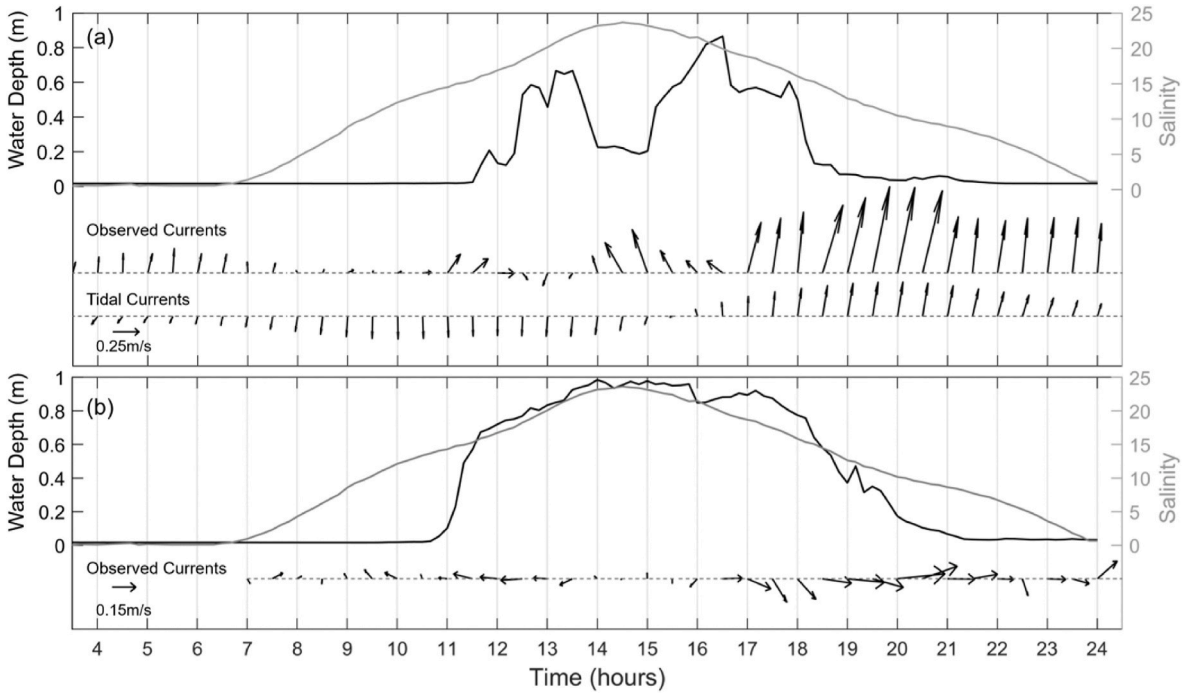

Fig. 9. Time series of observed salinity (black lines), water depth (grey lines), and both observed and tidal currents (black arrows) at the (a) surface and (b) bottom moorings on October 22.

the May survey, while it occurred at midday time during the October survey, reflecting the different timing of high tides across the two surveys. Aside from this timing difference, the presence of sea ice during winter may also indirectly mitigate the saltwater intrusion by hindering tidal propagation within YR estuary (Huang and Li, 2023).

4. Discussion

4.1. Estuarine regime of the Yellow River

In order to better understand the hydrodynamic regime of the Yellow River estuary, we attempt to position it in the Geyer and MacCready (2014) diagram, which is based on the freshwater Froude (Fr) and mixing (M) dimensionless numbers:

$$Fr = \frac{U_R}{\sqrt{\beta g S_0 H}} \tag{1}$$

$$M = \sqrt{\frac{C_D U_T^2}{\omega N_0 H^2}} \tag{2}$$

where U_R is the net river flow velocity approximated as the river volume flux divided by the estuarine section area, β is the coefficient of saline contraction [$\beta = 7.6 \times 10^{-4}$], g is the acceleration due to gravity [g = 9.81], S_0 is the ocean salinity [$S_0 = 32$], H is the water depth, C_D is the bottom drag coefficient, U_T is the amplitude of the tidal velocity, ω is the tidal frequency and $N_0 = \sqrt{\beta g s_0 / H}$ is the buoyancy frequency for maximum top-to-bottom salinity variation in an estuary. The former dimensionless parameter *Fr* represents the net velocity due to river flow scaled by the maximum possible frontal propagation speed, while the later M assesses the role of tidal mixing and the influence of stratification on the vertical mixing. The mapping of various estuaries onto the two-parameter Fr-M space (Fig. 10) have provided an effective means of discriminating different classes of estuaries. Salt-wedge estuaries are located near the top of the diagram with intense river forcing (i.e. high values of Fr). While time-dependent salt wedges such as the Fraser and Merrimack River reside in the upper-right corner, being strongly forced by tides and river flow. With moderate river velocities, strongly stratified and partially mixed estuaries take up the middle portion of the ordinate. Both regimes are characterized by well-developed gravitational circulations, representing high and low stratification conditions respectively. Fjord, with great depth that reduces both tidal and freshwater velocity scales, fall in the lower-left corner of the diagram. Well-mixed and SIPS (strain-induced periodic stratification) estuaries have relatively weak freshwater forcing and fall in the lower-right quadrant. Particularly, mixing timescale is shorter than the tidal timescale within SIPS estuaries, which exhibit periodic stratification mainly driven by tidal straining circulation (Simpson et al., 1990).

For the calculation of two parameters in the Yellow River, we considered H to be a characteristic value of 3 m in the river channel, and $C_D = 1.4 \times 10^{-3}$. Based on river runoff during the field campaigns, U_R estimation ranges from 0.32 to 0.62 m/s under low (~600 $m^3 s^{-1}$) to high (~1180 $m^3 s^{-1}$) discharge conditions for an estuarine section area about 1900 m^2. Therefore, Fr number should range from 0.37 to 0.73. The reference value of tidal velocity U_T is calculated from the surface current velocity series observed during the October campaign, based on a quasi-harmonic method (Pan et al., 2018). With U_T values from 0.1 to 0.3 ms^{-1} corresponding to tidal ranges from 0.4 to 2 m, the mixing parameter M ranges from 0.98 in neap tide to 1.4 in spring tide.

The YR estuary therefore falls in the upper right corner of the Fr and M parameter space (see the blue rectangle in Fig. 10), and is predominantly a time-dependent salt-wedge estuary. This kind of estuary features a strengthened stratification during the flood, and that weakens during the ebb tide as the turbulence develops in the full water column. During spring tides, this tidal asymmetry in stratification decreases as a result of enhanced mixing and reduced stratification during floods. The YR estuary's position on the diagram suggested that its dynamics may share some similarities with Fraser Estuary (Geyer and Farmer, 1989) and Merrimack rivers (Ralston et al., 2010), which are characterized by strong tidal and fluvial velocities. YR estuary seems to an outlier in these time-dependent salt-wedge estuaries, since it has a micro-tidal regime with a tidal range from 0.4 to 2 m. This may attribute to the very shallow depth within the estuary, which make it easier for the estuary to shift into a mixed status and thereby lead to a high M value.

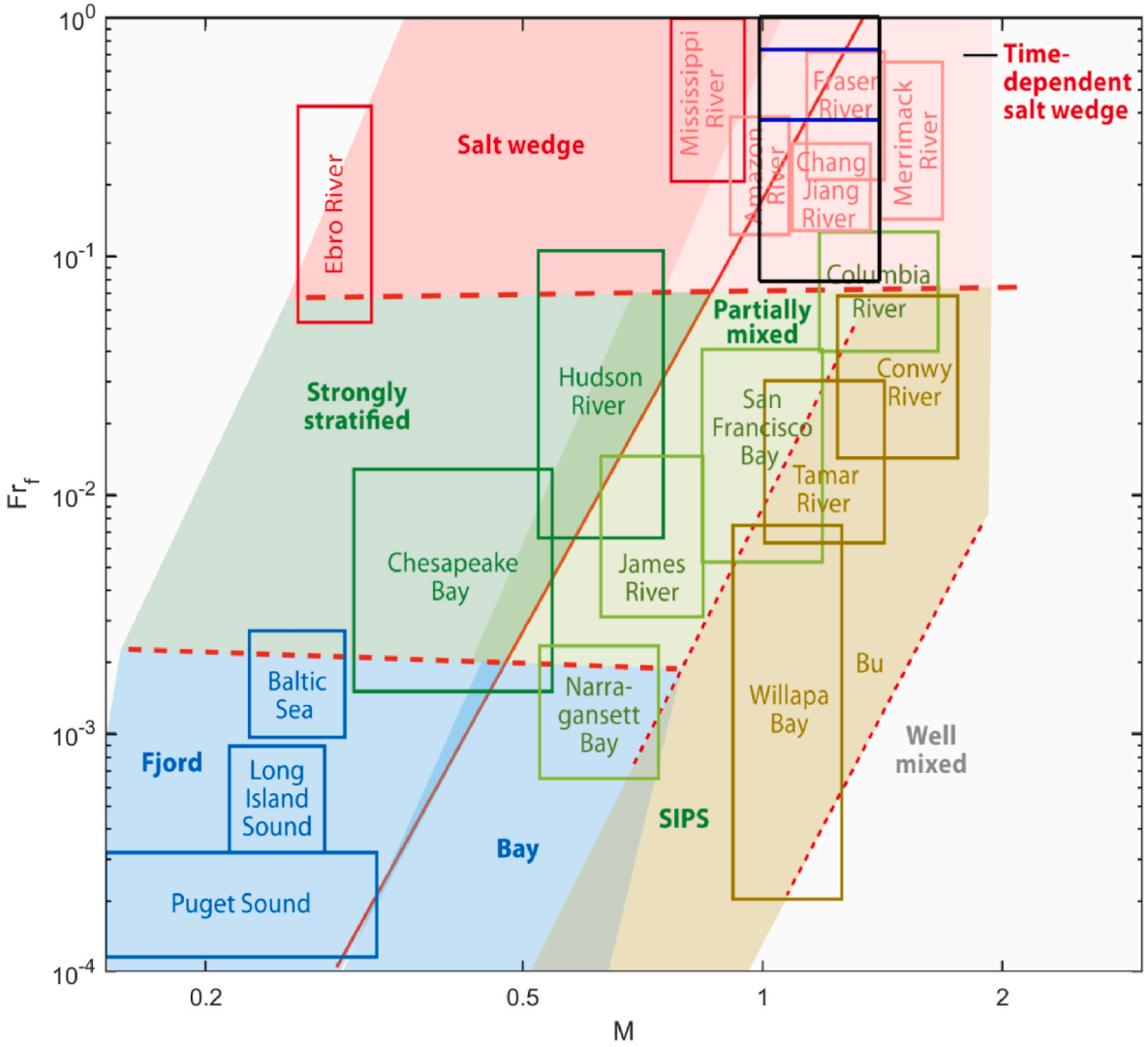

Fig. 10. Estuarine classification based on the freshwater Froude number and Mixing number, adapted from Fig. 6 of Geyer and MacCready (2014). The blue rectangle represents the Yellow River estuary based on observed data, while the black box indicates the region estimated using the runoff records throughout the year. (For interpretation of the references to colour in this figure legend, the reader is referred to the Web version of this article.)

4.2. *Effect of northeasterly winds on saltwater intrusion*

The water level series measured in spring and autumn recorded one and three distinct subtidal water level events, respectively. These events occurred on May 17 (Fig. 2c) and on October 18, 19, and 26 (Fig. 4c), which coincided closely with the dates when strong northeasterly winds prevailed. These episodic northeasterly winds were probably induced by the convergence of cold and warm air masses, which is closely related to convective activities in northern China (Liu et al., 2025). Given that the river discharge before and after these dates did not exhibit significant fluctuations, it is likely that these events were triggered by the strong northeasterly winds.

The events can be divided into two distinct stages, during which the impact of northeasterly winds on water levels and salinity in the river channel differed significantly. For instance, consider the event that occurred in spring. In the first stage, strong northeasterly winds prevailed on May 17 and generated a significant increment of water level (Fig. 2c), which led to increased peak salinity at the mooring station (Fig. 2d). This phase clearly demonstrated a marked enhancement of saltwater intrusion by the wind. The subsequent phase commenced as the wind shifted to a southerly direction on May 18. Although the water level was relatively high at approximately 21:00 on May 18, the surface salinity at the mooring station remained notably low, indicating minimal or no saltwater intrusion into the river channel on that date. Similar phenomena were observed from October 18 to October 20 and from October 26 to October 28. However, in contrast to the situation on May 18, saltwater was detected in the bottom layer of the mooring station on October 20 and 28, albeit with significantly lower salinity peaks and shorter durations. This suggests a relatively weak saltwater intrusion from the bottom layer following the strong northeasterly wind events.

The preceding analysis reveals that strong northeasterly winds can stimulate saltwater intrusion in the YRE during the timing of the wind, while subsequently impeding such intrusion for a day following the wind. The stimulation of saltwater intrusion by downwelling winds has also been documented in other estuarine systems, such as the Changjiang River (Zhu et al., 2020) and the Pearl River (Gong et al., 2018). However, the observed hindrance to saltwater intrusion following the wind appears to be a novel finding specific to the YRE. It is hypothesized that the substantial volume of freshwater accumulated in the river channel due to the wind flowed outward on the second day post-wind (October 20 and 27, Fig. 4e). This outward current impeded the inward tidal currents from external river channel, consequently hindering the transport of the surface saltwater into the river. However, the bottom salinity is induced by the inward bottom currents associated with tidal

movements, resulting in a continued, albeit weak, saltwater intrusion at the bottom layer. The reason of this disparity between the YR and the other major rivers in terms of mitigating saltwater intrusion following downwelling winds remains unclear, which will be further investigated through numerical modelling.

4.3. Influence of seasonal river discharge on saltwater intrusion

In addition to tidal and wind influences, river discharge also plays a critical role in modulating the saltwater intrusion in the river channel. Understanding the hydrological cycle of the Yellow River will help to facilitate the water resource management and salt intrusion mitigation within YR Estuary (Meng et al., 2025). The discharge of the Yellow River exhibits significant seasonal variation linked to monsoonal patterns, characterized by elevated discharge during the summer and autumn months (June to October) and reduced discharge during winter and spring (November to May). Notably, in the context of global warming, this monsoon-related seasonality may be intensified in the future, particularly with elevated summer discharge. Multiple studies (Li et al., 2024; Wang et al., 2025; Zhang and Wu, 2025) have demonstrated that the atmosphere's capacity to retain and transport moisture is increasing in Asia due to climate warming. This will amplify the moisture carried by summer monsoons and consequently lead to an increase in total summer precipitation. Apart from monsoonal influences, the spring YR discharge is also reported to be affected by the advanced green-up in the upper YR basin, which exacerbates local spring drought and consequently results in a lower runoff (Yu et al., 2025). Furthermore, the YR runoff has been regulated by the WSRS since 2002, resulting in notable short-term freshwater pulses in June or July.

Within 2023, the YR discharge varied from 167 m^3/s in February to 3690 m^3/s during the WSRS scheme in the early July, which is expected to cause substantial variations in the saltwater intrusion extent within YR estuary. However, during our spring survey in May 2023, the runoff ranged from 550 to 1250 m^3/s, significantly exceeding the average discharge in spring (~300 m^3/s) and comparable to that observed during the autumn survey. Consequently, the maximum intrusion lengths recorded during the spring and autumn surveys were relatively similar, measuring 3 km in spring and 4.5 km in autumn.

Despite these poorly contrasted runoff conditions during our measurements, the freshwater Froude number may provide some insights into how the estuary respond to its seasonality. The Fr value was estimated using records throughout the year 2023, and consequently the estuary could cover a wider behavioral region on the Geyer and MacCready (2014) diagram (see black box in Fig. 10). In the dry season with a typical runoff of ~200 m^3/s, Fr value could decrease to 0.08, indicating a more mixed system similar to the partially-mixed Columbia river. As river discharge increases up to 1200 m^3/s (with a Fr value equals 0.75), the influence of freshwater outflow becomes more important, leading to a salt-wedge regime under low tidal mixing conditions. Particularly, freshwater pulses during the WSRS scheme will increase Fr number to 2, a huge value that exceed all estuaries documented on the diagram. We therefore expect an absence of the salt-wedge due to strong river flow. The above analysis suggested that the seasonal variability of YR runoff has a pronounced impact on both saltwater intrusion and hydrodynamic regime within the YRE, which would require prospective scenarios with dedicated numerical modelling.

5. Conclusion

Based on in-situ measurement data and subsequent analysis, it can be concluded that tidal forces, wind patterns, and runoff significantly influenced saltwater intrusion within the YRE. Tidal dynamics affected saltwater intrusion in the YRE over multiple timescales. Due to its proximity to the amphidromic point of M_2 and S_2 tidal constituent, the tide in the estuary was predominantly diurnal, characterized by diurnal tidal currents. On the intratidal timescale, salinity variations in the surface and bottom layers featured distinct periodicities. Surface salinity exhibited semidiurnal changes, characterized by two peaks occurring around high water. A reasonable explanation for this phenomenon may be the combined effects of outward fluvial flow and inward tidal currents where surface salinity increased during flood tide but dropped when the inward tidal flow was overwhelmed by the outward movement of freshwater. While in the bottom layer, seawater was alternately driven into and out of the river channel by diurnal tidal currents, causing bottom salinity to vary diurnally with water level and reach its peak value at high tide. On the semi-month timescale, the water level within the YRE exhibited pronounced spring-neap variations associated with the 27.32-day cycle of lunar declination, referred to as a tropical month in astronomical terms. Spring tides occurred approximately two days following the maximum lunar declination, while neap tides coincided with its minimum value. Saltwater intrusion correlated with these spring-neap tidal variations, demonstrating a more substantial intrusion during spring tides compared to neap tides. Additionally, saltwater intrusion also responded to tidal changes over extended periods. Notably, the high tides, along with maximum saltwater intrusion, were observed at midnight in May and at midday in October during our survey in 2023. This temporal discrepancy is ascribed to the slight difference between the tidal cycle (K_1 tide) and the 24-h day, resulting in an approximate 12-h advancement from May to October.

The northeasterly wind emerged as a critical factor controlling saltwater intrusion within the YRE by modulating subtidal water levels. Strong northeasterly winds produced distinct subtidal water level increment, thereby greatly enhancing saltwater intrusion during their prevalence. However, minimal saltwater intrusion was observed on the day following the northeasterly wind event, particularly in the surface layer. This observation contrasts with findings from other large river systems such as the Changjiang and the Pearl River, suggesting a unique mechanism at play in the Yellow River. In the next phase of our research, this phenomenon will be further investigated using a three-dimensional primitive equation ocean model, the Princeton Ocean Model (POM). The model will be implemented on the whole Bohai Sea, and a finer resolution will be used in the Yellow River estuary and its adjacent waters with horizontal resolution of 100 m. Furthermore, the uneven distribution of runoff may contribute to notable seasonality in YRE saltwater intrusion. A more pronounced saltwater intrusion is expected during the spring and winter according to non-official accounts. Meanwhile, the estimations of the freshwater Froude number may indicate a transition from time-dependent salt-wedge to stagnant salt-wedge estuary conditions under large runoff. Nevertheless, these assumptions require further validation using hydrodynamic model beyond the observed data.

CRediT authorship contribution statement

Yunan Hu: Formal analysis, Investigation, Visualization, Writing – original draft. **Xinyu Guo:** Conceptualization, Writing – review & editing. **Yucheng Wang:** Investigation, Resources, Writing – review & editing. **Tao Zou:** Resources, Writing – review & editing. **Fangguo Zhai:** Writing – review & editing. **Xiaojie Yu:** Conceptualization, Funding acquisition, Investigation, Methodology, Supervision, Writing – review & editing.

Declaration of competing interest

The authors declare that they have no known competing financial interests or personal relationships that could have appeared to influence the work reported in this paper.

Acknowledgments

We are very grateful to the crews and captain involved in the surveys. This study was funded by the National Natural Science Foundation of China (42276010; 42149301, NORC2022-304). Y. Wang was supported

by Study on big data assimilation and fusion analysis model of super-resolution marine environment funded by the National Key Research and Development Program of China (No. 2021YFF0704002). X. Guo was supported by a Grant-in-Aid for Scientific Research (MEXT KAKENHI, grant number: 22H05206). This study was also partly supported by the Ministry of Education, Culture, Sports, Science and Technology, Japan (MEXT) to a project on Joint Usage/Research Center–Leading Academia in Marine and Environment Pollution Research (Lamer).

Data availability

Data will be made available on request.

References

Abood, K.H., 1974. Circulation in the hudson estuary. Ann. N. Y. Acad. Sci. 250, 38–111.
Chen, Y., Zuo, J., Zou, H., Zhang, M., Zhang, K., 2016. Responses of estuarine salinity and transport processes to sea level rise in the Zhujiang (Pearl River). Acta Oceanol. Sin. 35 (5), 38–48.
Gai, Y., Yu, M., Zhang, J., Qiao, S., 2025. Numerical simulation of salinity around yellow River Estuary during fish spawning period and its effect on spawning ground distribution. J. Ocean Univ. China 24, 886–896.
Gallo, M.N., Vinzon, S.B., 2005. Generation of overtides and compound tides in Amazon estuary. Ocean Dyn. 55, 441–448.
Geyer, W.R., Farmer, D.M., 1989. Tide-induced variation of the dynamics of a salt wedge estuary. J. Phys. Oceanogr. 19 (8), 1060–1072.
Geyer, W.R., MacCready, P., 2014. The estuarine circulation. Annu. Rev. Fluid Mech. 46, 175–197.
Goe, B.S., Dao, A., Brou, A.D., et al., 2025. Dynamics in salinity diffusion influenced by anthropogenic pressures and climate change: a case study of the Aghien lagoon (Abidjan, Côte d'Ivoire). Int. J. River Basin Manag. 1–14.
Gong, W., Lin, Z., Chen, Y., Chen, Z., Zhang, H., 2018. Effect of winds and waves on salt intrusion in the Pearl River estuary. Ocean Sci. 14 (1), 139–159.
Gong, W., Lin, Z., Zhang, H., Lin, H., 2022. The response of salt intrusion to changes in river discharge, tidal range, and winds, based on wavelet analysis in the Modaomen estuary. China. Ocean Coast Manag. 219, 106060.
Gong, W., Shen, J., 2011. The response of salt intrusion to changes in river discharge and tidal mixing during the dry season in the Modaomen Estuary, China. Cont. Shelf Res. 31, 769–788.
Hao, L., Sanada, A., Chi, B., Xiong, B., Maruya, Y., Yano, S., 2024. Long-term developments in seasonal hypoxia and response to climate change: a three-decade modeling study in the Ariake Sea, Japan. Sci. Total Environ. 929, 172471.
Huang, J., Xu, J., Gao, S., Lian, X., Li, J., 2015. Analysis of influence on the Bohai Sea Tidal system induced by coastline modification. J. Coast Res. 73 (1), 359–363.
Huang, B.Q., Li, X.M., 2023. Wave attenuation by sea ice in the Arctic marginal ice zone observed by spaceborne SAR. Geophys. Res. Lett. 50 e2023GL105059.
Ji, H., Pan, S., Chen, S., 2020. Impact of river discharge on hydrodynamics and sedimentary processes at yellow river Delta. Mar. Geol. 425, 106210.
Ji, H., Pan, S., Chen, S., Xu, C., Jiang, C., Fan, Y., 2018. Morphological variability of the active yellow river mouth under the new regime of riverine delivery. J. Hydrol. 564, 329–341.
Jia, W., Yi, Y., 2023. Numerical study of the water-sediment regulation scheme (WSRS) impact on suspended sediment transport in the yellow river Estuary. Front. Mar. Sci. 10, 1135118.
Kim, C., Park, K., 2012. A modelling study of water and salt exchange for a micro-tidal, stratified northern Gulf of Mexico Estuary. J. Mar. Syst. 96, 103–115.
Kujawa, R., Piech, P., 2022. Influence of water salinity on the growth and survivability of Asp Larvae Leuciscus aspius (Linnaeus, 1758) under controlled conditions. Animals 12, 2299.
Li, F., Lu, H., Wang, G., Qiu, J., 2024. Long-term capturability of atmospheric water on a global scale. Water Resour. Res. 60 (12) e2023WR034757.
Lin, X., Dröllner, M., Barham, M., Jing, L.Z., Jolivet, M., Liu, H., Guan, K., Hu, C., Chen, X., 2025. The Cenozoic evolution of the Yellow River. Earth Sci. Rev. 261, 104997.
Lin, X., Xu, Q., Barham, M., Jing, L.Z., Liu, H., Dröllner, M., Wu, Z., Li, Z., Hu, C., Chen, X., 2024. Tracing the source areas of detrital zircon and K-feldspar in the yellow river basin. Earth Sci. Rev. 251, 104718.
Liu, B., Peng, S., Liao, Y., Wang, H., 2019. The characteristics and causes of increasingly severe saltwater intrusion in pearl river Estuary. Estuar. Coast Shelf Sci. 220 (1), 54–63.
Liu, W., Wang, J., Zuo, H., et al., 2025. Spatiotemporal distribution and variation characteristics of convective activities in different climate zones in Northern China based on 25 years of satellite observations. Int. J. Climatol. 45 (10), e8908.
Liu, W.C., Chen, W.B., Cheng, R.T., Hsu, M.H., Kuo, A.Y., 2007. Modeling the influence of river discharge on salt intrusion and residual circulation in Danshuei River estuary, Taiwan. Cont. Shelf Res. 27 (7), 900–921.
Loc, H.H., Binh, D.V., Park, E., Sangam, S., Dung, T.D., Son, V.H., Truc, N.H.T., Mai, N.P., Seijger, C., 2021. Intensifying saline water intrusion and drought in the Mekong Delta: from physical evidence to policy outlooks. Sci. Total Environ. 757, 143919.
Lyu, H., Zhu, J., 2019. Impacts of tidal flat reclamation on saltwater intrusion and freshwater resources in the changjiang Estuary. J. Coast Res. 35 (2), 314–321.
Maccready, P., Geyer, W.R., 2010. Advances in estuarine physics. Ann. Rev. Mar. Sci 2 (1), 35–58.
Meng, G., Zhu, G., Jiao, Y., Qiu, D., Wang, Y., Lu, S., Li, R., Liu, J., Chen, L., Wang, Q., Huang, E., Li, W., 2025. Soil salinity patterns reveal changes in the water cycle of inland river basins in arid zones. Hydrol. Earth Syst. Sci. 29, 5049–5063.
Monismith, S.G., Kimmerer, W., Burau, J.R., Stacey, M.T., 2002. Structure and flow-induced variability of the subtidal salinity field in Northern San Francisco Bay. J. Phys. Oceanogr. 32, 3003–3019.
Neubauer, S., 2013. Ecosystem response of a tidal freshwater marsh experiencing salt water intrusion and altered hydrology. Estuary and Coast 36, 491–507.
Pan, H., Lv, X., Wang, Y., Matte, P., Chen, H., Jin, G., 2018. Exploration of tidal-fluvial interaction in the columbia river Estuary using S_TIDE. J. Geophys. Res., Oceans 123 (9), 6598–6619.
Payo-Payo, M., Bricheno, L.M., Dijkstra, Y.M., Cheng, W., Gong, W., Amoudry, L.O., 2022. Multiscale temporal response of salt intrusion to transient river and ocean forcing. J. Geophys. Res., Oceans 127 e2021JC017523.
Perales-Valdivia, H., Sanay-González, R., Valle-Levinson, A., 2018. Effects of tides, wind and river discharge on the salt intrusion in a microtidal tropical estuary. Regional Study of Marine Science 24, 400–410.
Pugh, D.T., 1987. Tides, Surges and Mean Sea Level. John Wiley and Sons, New York, p. 472.
Qin, H., Shi, H., Gai, Y., Qiao, S., Li, Q., 2023. Sensitivity analysis of runoff and wind with respect to yellow river Estuary salinity plume based on FVCOM. Water 15 (7), 1378.
Qiu, C., Zhu, J., Gu, Y., 2012. Impact of seasonal tide variation on salt intrusion in Changjiang river estuary. Chin. J. Oceanol. Limnol. 30 (2), 342–351.
Qiu, C., Zhu, J., 2015. Assessing the influence of sea level rise on salt transport processes and estuarine circulation in the Changjiang River estuary. J. Coast Res. 31 (3), 661–670.
Ralston, D.K., Geyer, W.R., Lerczak, J.A., 2010. Structure, variability, and salt flux in a strongly forced salt wedge estuary. J. Geophys. Res., Oceans 115, C06005.
Ralston, D.K., Talke, S., Geyer, W.R., Al-Zubaidi, H.A.M., Sommerfield, C.K., 2019. Bigger tides, less flooding: effects of dredging on barotropic dynamics in a highly modified estuary. J. Geophys. Res., Oceans 124 (1), 196–211.
Savenije, H.H.G., 2012. Salinity and Tides in Alluvial Estuaries. Delft University of Technology, Delft, The Netherland, p. 163.
Simpson, J.H., Brown, J., Matthews, J., Allen, G., 1990. Tidal straining, density currents, and stirring in the control of estuarine stratification. Estuaries 13, 125–132.
Tully, K., Gedan, K., Epanchin-Niell, R., Strong, A., Bernhardt, E.S., BenDor, T., Mitchell, M., Kominoski, J., Jordan, T.E., Neubauer, S.C., Weston, N.B., 2019. The invisible flood: the chemistry, ecology, and social implications of coastal saltwater intrusion. Bioscience 69 (5), 368–378.
Veerapaga, N., Azhikodan, G., Shintani, T., Iwamoto, N., Yokoyama, K., 2019. A three-dimensional environmental hydrodynamic model, Fantom-refined: validation and application for saltwater intrusion in a meso-macrotidal estuary. Ocean Model. 141, 101425.
Wang, J., Li, L., He, Z., Kalhoro, N.A., Xu, D., 2019. Numerical modelling study of seawater intrusion in Indus River Estuary, Pakistan. Ocean Eng. 184, 74–84.
Wang, Q., Guo, X., Takeoka, H., 2008. Seasonal variations of the Yellow River plume in the Bohai sea: a model study. J. Geophys. Res., Oceans 113 (C8).
Wang, Q., Liu, Y., Zhu, G., Lu, S., Chen, L., Jiao, Y., Li, W., Li, W., Wang, Y., 2025. Regional differences in the effects of atmospheric moisture residence time on precipitation isotopes over Eurasia. Atmos. Res. 314, 107813.
Wang, Y., Liu, Z., Gao, H., Ju, L., Guo, X., 2011. Response of salinity distribution around the Yellow River mouth to abrupt changes in river discharge. Cont. Shelf Res. 31 (6), 685–694.
Wei, B.C., Wen, C.L., Ming, H.H., 2015. Modeling assessment of a saltwater intrusion and a transport time scale response to sea-level rise in a tidal estuary. Environ. Fluid Mech. 15, 491–514.
Wong, K.C., Lu, X., 1994. Low-frequency variability in Delaware's inland bays. J. Geophys. Res., Oceans 99 (C6), 12683–12695.
Wu, H., Zhu, J., Choi, B.H., 2010. Links between saltwater intrusion and subtidal circulation in the Changjiang Estuary: a model-guided study. Cont. Shelf Res. 30, 1891–1905.
Xia, C., Liu, G., Xia, H., Jiang, F., Meng, Y., 2021. Influence of saline intrusion on the wetland ecosystem revealed by isotopic and hydrochemical indicators in the Yellow River Delta, China. Ecol. Indic. 133, 108422.
Xing, Y., Ai, C., Jin, S., 2013. A three-dimensional hydrodynamic and salinity transport model of estuarine circulation with an application to a macrotidal estuary. Appl. Ocean Res. 39, 53–71.
Yu, L., Liu, Y., Shen, M., Yu, Z., Li, X., Liu, H., Lyne, V., Jiang, M., Wu, C., 2025. Extreme hydroclimates amplify the biophysical effects of advanced green-up in temperate China. Agric. For. Meteorol. 363, 110421.
Yu, X., Guo, X., Gao, H., Zou, T., 2021. Upstream extension of a bottom-advected plume and its mechanism: the case of the yellow River. J. Phys. Oceanogr. 51, 2351–2371.
Zhang, H., Chen, X., Luo, Y., 2016. An overview of ecohydrology of the Yellow River delta wetland. Ecohydrol. Hydrobiol. 16 (1), 39–44.
Zhang, Y., Wu, X., 2025. Global space-time patterns of sub-daily extreme precipitation and its relationship with temperature and wind speed. Environ. Res. Lett. 20, 084019.
Zhao, Y., Lu, M., Chen, D., Zhang, L., 2024. Understanding the weakening patterns of inner Tibetan Plateau vortices. Environ. Res. Lett. 19, 064076.
Zhu, J., Cheng, X., Li, L., Wu, H., Gu, J., Lyu, H., 2020. Dynamic mechanism of an extremely severe saltwater intrusion in the Changjiang Estuary in February 2014. Hydrol. Earth Syst. Sci. 24, 5043–5056.